Journal of Electrical Engineering & Technology (2025) 20:567–574
https://doi.org/10.1007/s42835-024-01987-5

ORIGINAL ARTICLE

Study on Electromagnetic Performance of Skewed Permanent Magnet Axial Flux Permanent Magnet Synchronous Motor

Junhong Wang[2] · Zengjin Xu[1] · Zuoxia Xing[2] · Yang Liu[2] · Wei Ji[2]

Received: 28 February 2024 / Revised: 9 July 2024 / Accepted: 23 July 2024 / Published online: 17 August 2024

Abstract
Axial flux motors have more advantages than radial flux motors in terms of volume, torque to inertia ratio, efficiency and power density. However, when using axial flux permanent magnet synchronous motor (AFPMSM) as hub motor for electric vehicles, their torque ripples it is a thorny problem that affects its development. It is a common method to reduce the torque ripple by weakening the cogging torque. This paper studies the impact of permanent magnet deflection on motor torque ripple, efficiency and other aspects in the absence of cogging torque, that is, no stator core. Finite element simulation results show that the permanent magnet deflection of 10° is the optimal deflection angle. Currently, the electromagnetic torque pulsation is smallest, the radial air gap magnetic density waveform is closest to the sine wave, the magnetic induction intensity is the largest, and the efficiency is highest. This research result provides an effective method for reducing torque ripple of in-wheel motors.

Keywords Axial flux permanent magnet synchronous motor (AFPMSM) · Permanent magnet skew · Torque ripple · Finite element simulation

1 Introduction

Excessive torque pulsation of the electric vehicle wheel hub motor will cause large vibration and noise during vehicle driving, affecting driving comfort and stability [1, 2]. Measures such as increasing the number of motor poles, optimizing the motor magnetic field distribution, and slot less cores can reduce torque ripple [3–5]. Although after improvement and optimization, the torque pulsation of modern in-wheel motors has been alleviated to a certain extent, there is still a certain amount of torque pulsation [6]. In order to minimize the torque ripple without increasing the overall mass of the motor, this paper selects the AFPMSM as the research object [7, 8].

Since the AFPMSM has no reduction gear, the rotation speed is lower than that of the radial flux motor [9, 10]. When the output power is the same, the mass and volume are half of the radial flux motor [11]. Moreover, the AFPMSM uses magnetic force to generate torque, and its torque is proportional to the cube of the rotor radius [12–14]. In contrast, the torque of a radial flux motor is proportional to the square of the rotor radius [15]. AFPMSM therefore have a higher torque-to-weight ratio. Since the torque is proportional to the cube of the rotor radius, the rotor core of the AFPMSM can be better utilized and has higher power density [16, 17]. This means that the AFPMSM can produce greater torque in the same space [18]. In addition, the structural symmetry of the axial flux permanent magnet motor solves the problems of space limitations and efficiency of traditional wheel hub motors [7, 19].

In [20], a system-level design optimization method based on the actual operating environment is proposed. In [21, 22], multi-objective optimization was proposed based on

✉ Zengjin Xu
zengjin_xu@sut.edu.cn

Junhong Wang
1026800778@qq.com

Zuoxia Xing
xingzuox@163.com

Yang Liu
yangliu9611@163.com

Wei Ji
782572921@qq.com

[1] School of Electrical Engineering, Shenyang University of Technology, Shenyang, China

[2] School of Electrical Engineering, Shenyang University of Technology, Shenyang, China

sequential subspace optimization and climbing algorithm. These research studies mainly focus on the comprehensive optimization of motor efficiency and electromagnetic performance using different multi-objective optimization methods. In [23], by considering the non-uniform distribution of axial air gap magnetic flux density, an optimal step deflection method of a cantilevered PMSM with a rotor axial length greater than the stator axial length is proposed to reduce torque ripple. However, the study only analyzed the situation where the ratio of the air gap magnetic flux density reduction length to the entire axial length of the motor is 4% and 10%. Other situations were not analyzed, which has great limitations. In [24] uses the double slope method to design the permanent magnet into a multiplicative waveform to reduce the torque ripple. On the basis of the traditional two-dimensional structure, the permanent magnet is three-dimensionally deflected relative to the Z-axis direction, which undoubtedly increases the Manufacturing difficulty. In [25] skewed the magnets in V and However, the degree of V- and X-shaped skew has not been studied in detail. Previous studies have treated permanent magnets with an iron core to reduce torque ripple. This paper chose to design a 28kW dual-rotor single-stator AFPMSM without an iron core to study the deflection of the permanent magnet at this time. The impact on the no-load and load conditions of the motor at different tilt angles.

2 Motor Design

2.1 Motor Structure and Magnetic Circuit Selection

According to the topological structure, AFPMSM can be divided into: single-stator single-rotor, double-rotor single-stator, double-stator single-rotor, and multiple-stators multiple-rotors [26–28]. Among them, the double-rotor single-stator adds a rotor based on the single-stator single-rotor. The two rotors are arranged on both sides of the stator, and the windings on the stator interact with the two rotors at the same time. Moreover, since the rotor disk is symmetrically distributed on both sides of the stator disk, a double air gap structure can be formed, effectively reducing the generation of leakage magnetic flux. Magnetic flux leakage is one of the energy losses during motor operation. Reducing magnetic flux leakage can improve the efficiency of the motor. The symmetrical distribution of the rotor disk can also avoid the problem of axial force imbalance and reduce the vibration and noise generated when the motor is running. In addition, this structure also improves the utilization of permanent magnets, so this paper chooses a double-rotor single-stator structure.

The topological structure of double-rotor and single-stator can be divided into two types: stator with iron core and stator without iron core [7]. In traditional motors with a stator core, the magnetic field is transmitted between the rotor and the stator through the iron core. However, the iron core structure can cause problems such as magnetic circuit saturation, resulting in low efficiency. The stator coreless structure improves the efficiency of the motor by changing the magnetic circuit of the motor to solve problems such as magnetic circuit saturation and torque pulsation. Moreover, the ironless core also reduces the mass of the motor, making the motor lighter and more suitable for in-wheel motors.

The dual-rotor single-stator structure can be divided into the NN structure as shown in Fig. 1a and the NS structure as shown in Fig. 1b according to the magnetic pole arrangement. The main difference lies in whether the magnetic circuit passes through the stator yoke [29–31]. The NS arrangement has no interference from the stator yoke magnetic circuit. The magnetic circuit is relatively open. The magnetic induction lines pass through the permanent magnet, pass through the air gap and winding, pass through the air gap on the other side, and enter the permanent magnet. This structure has a large magnetic energy dispersion range and relatively small stray losses. In the NN arrangement, due to the existence of the stator yoke magnetic circuit, the magnetic flux is more concentrated. The magnetic flux lines pass out from the permanent magnet, pass through the air gap, enter the stator yoke, and pass out of the air gap on the same side into the phase. Adjacent to permanent magnets, this structure has a short magnetic circuit, small magnetic resistance, and high magnetic circuit transmission efficiency, but there is a certain magnetic pressure and stray loss. Since this paper chooses a stator less core structure, the NS arrangement is selected, and the insulation performance of the fixed winding is improved, and the winding is plastic-sealed into a thin disk with epoxy resin.

2.2 Motor Model Building

According to the formula of the main dimensions of the AFPMSM, the size of the motor can be calculated as shown in Table 1.

Since the permanent magnet needs to be tilted at different angles, it cannot be directly parameterized using the RMxprt module in Maxwell. This paper builds the model according

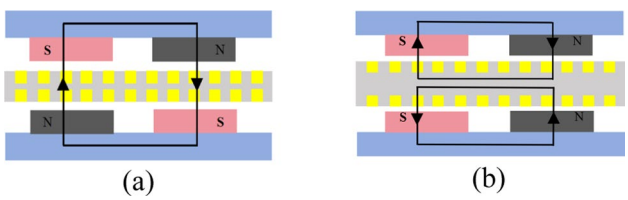

Fig. 1 Double-rotor single-stator structure. **a** NS structure. **b** NN structure

Table 1. Motor parameters

Parameter	Value
rated power/kW	28
rated voltage/V	380
rated frequency/Hz	400
rated speed/rpm	3000
rotor outer diameter/mm	382
rotor inner diameter/mm	218
rotor core thickness/mm	15
Permanent magnet thickness/mm	10
number of pole pairs	8
pole embrace	0.7
number of parallel branches	2
parallel winding number	2
winding connection method	Y
permanent magnet selection	NdFe30

to the motor size in SolidWorks and then imports it into Maxwell 3D. The final motor model is shown in Fig. 2. In order to reduce the calculation amount and calculation time and improve the simulation efficiency. The motor model is first segmented in the static magnetic field, and the segmentation results are shown in Fig. 3. Then the segmentation results are imported into the transient field for simulation.

2.3 Permanent Magnet Skewed Design

Permanent magnet deflection design refers to the deflection treatment of the permanent magnets at a certain angle to achieve a specific magnetic field distribution during the permanent magnet design process. The motor designed in this paper uses 16 permanent magnets with 8 pairs of poles. The central angle occupied by the magnet is 22.5°. Considering that the polar arc coefficient is 0.7, both sides of the permanent magnet are reduced by 7.50 mm. The permanent magnets are skewed 0–22°, among which 0°, 5°, 10°, 15°,

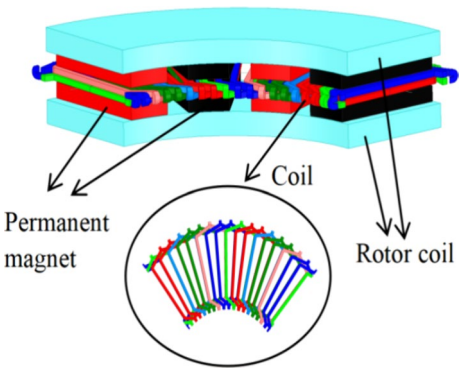

Fig. 2 Motor 3D model

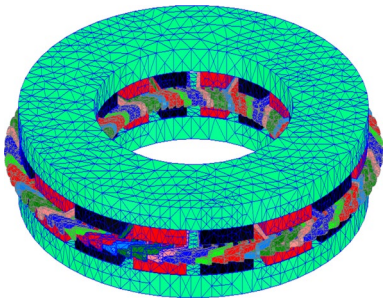

Fig. 3 Static magnetic field meshing model

and 20° are proposed. Other results are shown in Table 2 Comparison of performance indicators of permanent magnet deflection at different angles. Fig. 4 is the operation of the permanent magnet deflection of 5°. The model of the permanent magnet deflection of 0°, 5°, 10°, 15°, and 20° is shown in Fig. 5.

3 Analysis of Finite Element Simulation Results

3.1 No-load Condition Analysis

From Fig. 6, the no-load electromagnetic torque increases first and then decreases with the skew angle of the permanent magnet. At 10°, the pulsation is the smallest, and the pulsation coefficient is 1.92%, which is the same as when there is no skew. Compared with 19.46%, it decreased by 17.54%. The pulsation increases sharply from 15° to 20°. When the permanent magnet rotates, the direction of the magnetic field is no longer completely perpendicular to the direction of motion of the rotor, but will produce a certain tilt angle, like the use of a Halbach array for permanent magnets. This results in the permanent magnet's magnetic force on the rotor being inconsistent at different positions. This uneven magnetic force will cause torque pulsation. In this paper, skewing 5°, 15°, and 20° is unreasonable, resulting in greater torque ripple than no skew. Skewing 10° is a more reasonable angle, so that The torque ripple is reduced. When the deflection angle matches the rotor movement speed, magnetic field distribution and other factors, the magnetic force at different positions can be ripple.

3.2 Load Condition Analysis

The load condition can apply current excitation or voltage excitation to the motor. This paper chooses to apply current excitation because current excitation can more directly control the working state of the motor. The output power and speed of the motor are directly related to its

Table 2 Comparison of performance indicators of permanent magnets with different angles of skew

Skew angles(°)	No-load electromagnetic torque ripple coefficient(%)	Maximum value of load magnetic density cloud chart(T)	Load induced electromotive force (V)	Efficiency (%)
0	19.46	1.4979	365.11	91.3
1	21.79	1.4991	364.39	91.46
2	22.54	1.4998	362.08	91.62
3	27.92	1.5202	360.13	91.78
4	28.11	1.5547	359.86	91.94
5	28.14	1.5755	359.46	92.10
6	27.64	1.5842	358.80	92.62
7	10.70	1.6203	350.60	93.14
8	5.38	1.6700	348.05	93.66
9	2.33	1.7288	342.67	94.18
10	1.92	1.7485	338.47	94.70
11	1.97	1.7480	337.83	93.66
12	3.33	1.7064	330.06	92.62
13	5.78	1.6441	326.77	91.58
14	9.16	1.5580	310.95	90.54
15	9.38	1.5091	309.90	89.50
16	14.45	1.5486	301.04	89.48
17	17.66	1.5922	299.65	88.86
18	20.70	1.6320	290.44	88.54
19	22.51	1.6591	275.09	88.22
20	30.23	1.6675	273.80	87.90
21	38.59	1.7080	271.22	87.87
22	44.36	1.7309	269.08	87.02

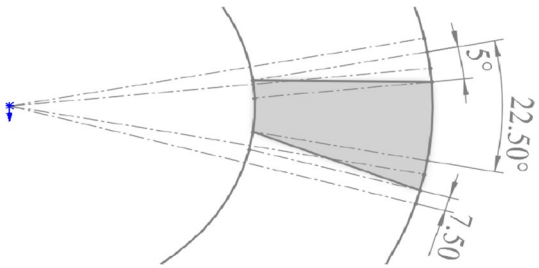

Fig. 4 Skew angle design

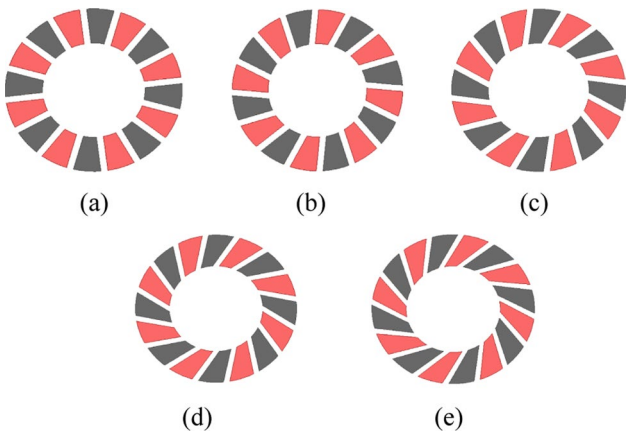

Fig. 5 Skewed permanent magnets at different angles. **a** Skew 0°. **b** Skew 5°. **c** Skew 10°. **d** Skew 15°. **e** Skew 20°

current, and precise control of the motor can be achieved by controlling the current. The applied current excitation is as shown in Equation (1)

$$\begin{cases} Iqrms^{*}sqrt(2)\sin\left(2^{*}\pi\dfrac{3000}{60}*8*time\right) \\ Iqrms^{*}sqrt(2)\sin\left(2^{*}\pi\dfrac{3000}{60}*8*time-2\dfrac{\pi}{3}\right) \\ Iqrms^{*}sqrt(2)\sin\left(2^{*}\pi\dfrac{3000}{60}*8*time+2\dfrac{\pi}{3}\right) \end{cases} \quad (1)$$

In the formula, *Iqrms* is the effective value of current.

Fig. 7 shows that the load speed has not changed significantly. As time goes on, the speed gradually stabilizes at 3000 rpm. The skew of the permanent magnet will cause the magnetic field of the permanent magnet to not completely coincide with the stator magnetic field, resulting in the displacement of the torque generation position.

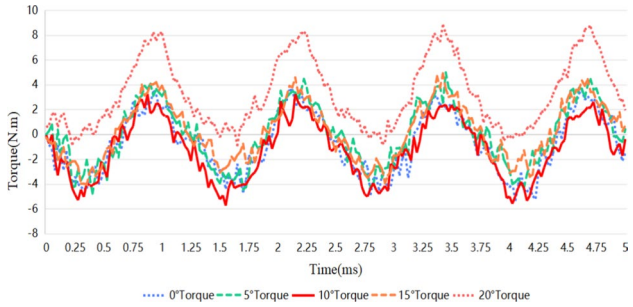

Fig. 6 Electromagnetic torque

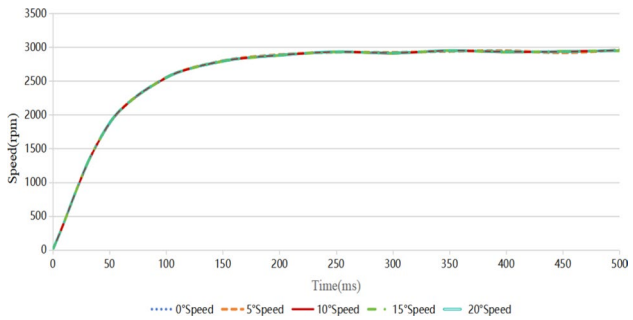

Fig. 7 Speed

However, the relationship between speed and torque is not linear, so the influence of deviation on speed is relatively small. The torque fluctuation caused by the skew may cause vibration and noise, but it will not directly affect speed.

When the permanent magnet is skewed, the magnetic field line will be distorted, resulting in uneven distribution of the magnetic field. The uneven magnetic field will cause the magnetic field line density to be unevenly distributed, resulting in uneven changes in magnetic flux. According to Faraday's law of electromagnetic induction and Ampere's loop law, this will lead to the weakening of the magnetic induction intensity in a specific area, and the distortion of the magnetic field line may also make the magnetic field more concentrated. This results in increased magnetic induction in specific areas. Changes in magnetic flux lead to changes in magnetic induction intensity. As shown in Fig. 8, the magnetic induction intensity increases from 0° to 10°, and then decreases from 10° to 20°. It can be observed that when skewed by 10°, the magnetic induction intensity is greater than other angles. Although the magnetic density map turns red at this time, it does not exceed the saturation magnetic induction intensity of the magnet material neodymium iron boron but works near the saturation point.

As the skew angle of the permanent magnet increases from 0° to 20°, the magnetic field inhomogeneity increases, resulting in a decrease in the magnetic induction intensity,

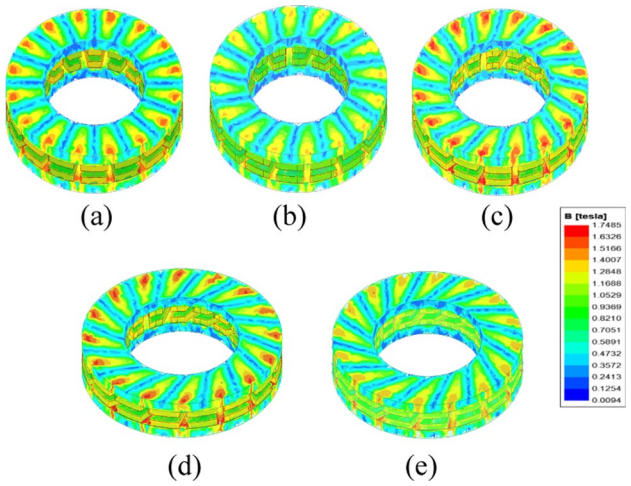

Fig. 8 Magnetic density cloud map. **a** Skew 0°. **b** Skew 5°. **c** Skew 10°. **d** Skew 15°. **e** Skew 20°

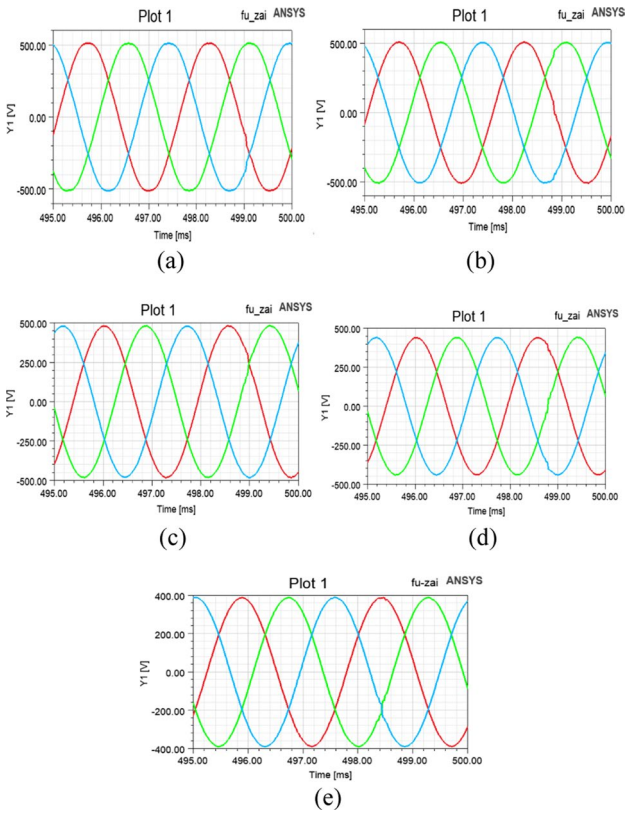

Fig. 9 Induced electromotive force. **a** Skew 0°. **b** Skew 5°. **c** Skew 10°. **d** Skew 15°. **e** Skew 20°

corresponding to a decrease in the induced electromotive force shown in Fig. 9.

As shown in Fig. 10, when the skew Angle of permanent magnet is 10°, the radial air gap magnetic density is overall closest to the sine wave compared with other skew

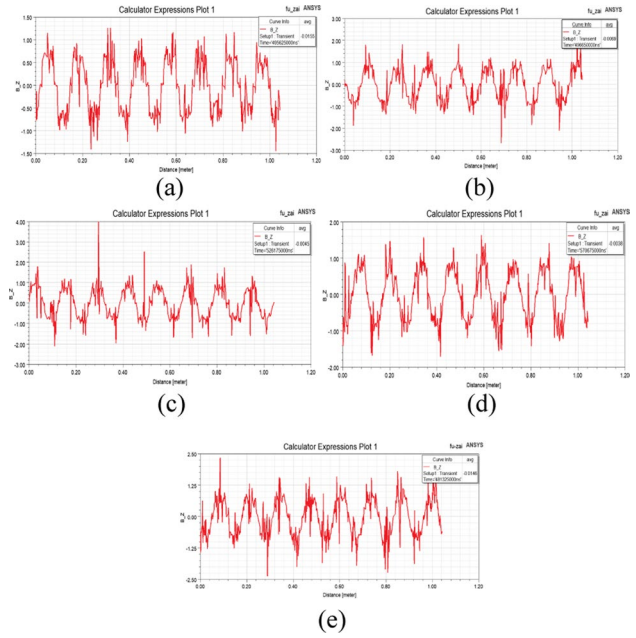

Fig. 10 Radial air gap magnetic density. **a** Skew 0°. **b** Skew 5°. **c** Skew 10°. **d** Skew 15°. **e** Skew 20°

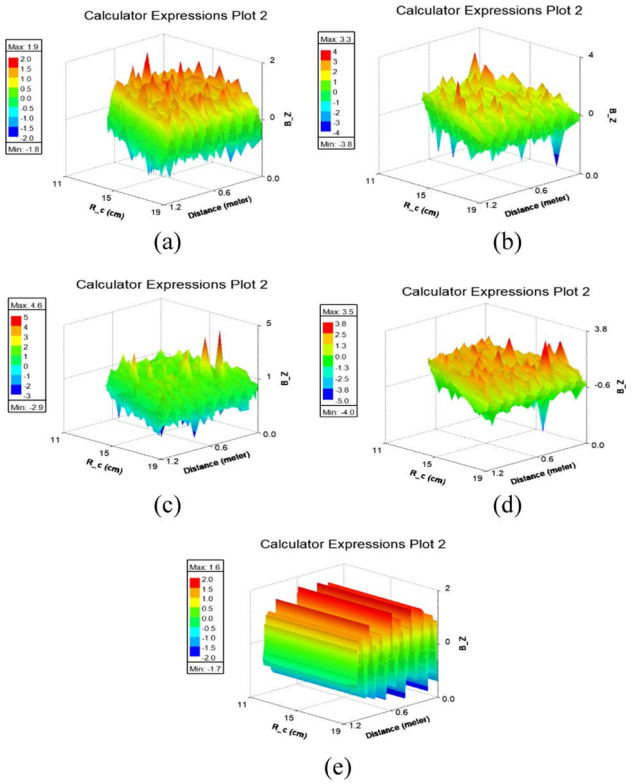

Fig. 11 Three-dimensional air gap magnetic density cloud map. **a** Skew0°. **b** Skew 5°. **c** Skew 10°. **d** Skew 15°. **e** Skew 20°

angles overall. The radial air gap magnetic density is close to sine wave, which can reduce the fluctuation of magnetic force, reduce the generation of vibration and noise, make the magnetic linkage and current of the motor more stable, and reduce the reluctance loss and iron loss. Improve motor performance and improve motor efficiency.

Because AFPMSM not only have radial air gap magnetic flux density but also axial flux density, only analyzing radial air gap magnetic flux density cannot better illustrate the air gap magnetic flux density of the motor. Therefore, it is necessary to analyze the three-dimensional cloud map of air gap magnetic flux density, as shown in Fig. 11. When the skew angle is 10°, the corresponding air gap magnetic flux density is the most uniform. The reason for the particularly large air gap magnetic flux density in several places in the magnetic flux cloud map is that the magnetic field in some areas is uneven due to the skew of the magnet, relatively concentrated, resulting in a higher air gap magnetic density. In areas with high magnetic density, the magnetic field strength is also high. According to simulation results, the load magnetic field strength corresponding to a skew of 10° is indeed the highest, which is consistent with theory.

Compared with the traditional stator core motor, the ironless motor has great advantages in efficiency and quality, the permanent magnet is skewed on the basis of the no core, the loss is reduced, the output power is increased, and the motor efficiency is improved, Fig. 12 shows that the permanent magnet skew angle is too large to reduce the motor efficiency, and even lower than the non-skewed efficiency, when the permanent magnet is skewed by 10°, the motor efficiency is the highest, reaching 94.7%, which is 3.4% higher than the non-skewed efficiency.

4 Conclusion

The purpose of this paper is to reduce torque ripple, improve air gap magnetic flux density, and enhance magnetic induction strength by skewing the permanent magnet of a dual rotor single stator axial flux coreless permanent magnet synchronous motor at different angles. This motor is used as the

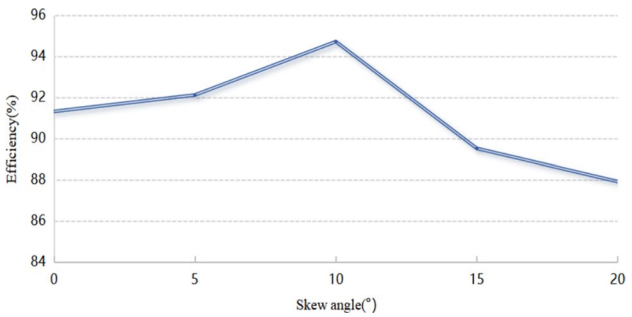

Fig. 12 Motor efficiency

hub motor for electric vehicles to solve the problem of large torque ripple in hub motors. The design and finite element simulation of AFPMSM were carried out using SolidWorks and Maxwell software. The research results showed that when the permanent magnet was skewed 10°, the torque ripple was the smallest, the air gap magnetic flux density was the highest, the magnetic induction intensity was the highest, and the efficiency was the highest, which increased by 3.4% compared to when it was not skewed. This study provides an effective method for reducing torque ripple in electric vehicle hub motors.

Acknowledgements This work was supported by Liaoning Revitalization Talents Program (XLYC2008005).

Declarations

Conflict of interest The authors declare that we have no competing financial interests or personal relationships that could have appeared to influence the work reported in this paper.

References

1. Boduroglu A, Gulec M, Demir Y, Yolacan E, Aydin M (2019) A new asymmetric planar V-shaped magnet arrangement for a linear PM synchronous motor. IEEE Trans. Magn. 55(7):1–5
2. Arabul FK, Senol I, Oner Y (2020) Performance analysis of axial-flux induction motor with skewed rotor. Energies 13(19):4991
3. Polat M, Yildiz A, Akinci R (2021) Performance analysis and reduction of torque ripple of axial flux permanent magnet synchronous motor manufactured for electric vehicles. IEEE Trans. Magn. 57(7):1–9
4. Jia L, Lin M, Le W, Li N, Kong Y (2020) Dual-skew magnet for cogging torque minimization of axial flux PMSM with segmented stator. IEEE Trans. Magn. 56(2):1–6
5. Ahmad N, Khan F, Ali H, Jshaq S, Sulaiman E (2019) Outer rotor wound field flux switching machine for in-wheel direct drive application. IET Elect. Power Appl. 13(6):757–765
6. Zhao X, Niu S, Zhang X, Fu W (2020) Design of a new relieving DC-saturation hybrid reluctance machine for fault-toleration in-wheel direct drive. IEEE Trans. Ind. Electron. 67(11):9571–9581
7. Wang C, Han J, Zhang Z, Hua Y, Gao H (2022) Design and optimization analysis of coreless stator axial-flux permanent magnet in-wheel motor for unmanned ground vehicle. IEEE Trans. Transp. Electrific. 8(1):1053–1062
8. Aydin M, Huang S, Lipo TA (2006) Torque quality and comparison of internal and external rotor axial flux surface-magnet disc machines. IEEE Trans. Ind. Electron. 53(3):822–830
9. Hang Peng, Chen X (2021) Towards autonomous driving: review and perspectives on configuration and control of four-wheel independent drive/steering electric vehicles. Multidiscip Digit Publ Inst 10(8):184
10. Peng B, Wang X, Zhao W, Ren J (2019) Study on shaft voltage in fractional slot permanent magnet machine with different pole and slot number combinations. IEEE Trans. Magn. 55(6):1–5
11. Kim K-C (2014) A novel method for minimization of cogging torque and torque ripple for interior permanent magnet synchronous motor. IEEE Trans. Magn. 50(2):793–6
12. Zhao W, Lipo TA, Kwon B-I (2014) Material-efficient permanent magnet shape for torque pulsation minimization in SPM motor for automotive applications. IEEE Trans. Ind. Electron. 61(10):5779–5787
13. Du ZS, Lipo TA (2020) Reducing torque ripple using axial pole shaping in interior permanent magnet machines. IEEE Trans. Ind. Appl. 56(1):148–157
14. Chen Q, Xu G, Zhai F, Liu G (2020) A novel spoke-type PM motor with auxiliary salient poles for low torque pulsatuion. IEEE Trans. Ind. Electron. 67(6):4762–4773
15. Lai C, Feng G, Mukherjee K, Loukanov V, Kar NC (2018) Torque ripple modeling and minimization for interior PMSM considering magnetic saturation. IEEE Trans. Power Electron. 33(3):2417–2429
16. Li N, Fu X, Zhu J, Lin M, Yang G, Hao L (2019) Hybrid-excited series permanent magnet axial field flux switching memory machine. IEEE Trans. Appl. Supercond. 29(2):1–5
17. Jahns TM, Kliman GB, Neumann TW (1986) Interior permanent-magnet synchronous motors for adjustable-speed drives. IEEE Trans. Ind. Appl. 1A-22(4):738–747
18. Wu D, Xiang Z, Zhu X, Quan L, Jiang M, Liu Y (2021) Optimization design of power factor for an in-wheel vernier pm machine from the perspective of air-gap harmonic modulation. IEEE Trans. Ind. Electron. 68(10):9265–9276
19. Ahmad N, Khan F, Ali H, Ishaq S, Sulaiman E (2019) Outer rotor wound field flux switching machine for in-wheel direct drive application. IET ELect. Power Appl. 13(6):757–765
20. Sun X, Shi Z, Cai Y, Lei G, Guo Y, Zhu J (2020) Driving-cycle-oriented design optimization of a permanent magnet hub motor drive system for a four-wheel-drive electric vehicle. IEEE Trans. Transp. Electrific. 6:1115
21. Sun Xiaodong, Naixi Xu, Yao Ming (2023) Sequential subspace optimization design of a dual three-phase permanent magnet synchronous hub motor based on NSGA III. IEEE Trans. Transp. Electrific. 9(1):622–630
22. Jin Zhijia, Sun Xiaodong, Chen Long, Yang Zebin (2022) Robust multi-objective optimization of a 3-pole active magnetic bearing based on combined curves with climbing algorithm. IEEE Trans. Ind. Electron. 69(6):5491–5501
23. P. T. Luu, J. -Y. Lee, W. Hwang and B. -C. Woo, 2018 "Cogging Torque Reduction Technique by Considering Step-Skew Rotor in Permanent Magnet Synchronous Motor,"In: 2018 21st International Conference on Electrical Machines and Systems. Jeju. Korea
24. D. Sato, R. Maejima, W. Kitagawa and T. Takeshita, "Cogging Torque Reduction by Using Double Skew of Permanent Magnets in Axial Gap Motor,"In: 2022 International Conference on Electrical Machines, Valencia, Spain, September 2022.
25. K. Kurihara, H. Yoshino and K. Shimauchi, "Surface Permanent Magnet Motors with Complicated Permanent Magnet Shapes Formed by Binder-Less Net Shaping Process,"In: 2018 21st International Conference on Electrical Machines and Systems, Jeju, Korea, October 2018.
26. Galioto SJ, Reddy PB, EL-Refaie AM, Alexander JP (2015) Effect of magnet types on performance of high-speed spoke interior-permanent magnet machines dedigned for traction applications. IEEE Ind. Appl. 51(3):2148–2160
27. Koo B, Kim J, Nam K (2021) Halbach array PM machine design for high speed dynamo motor. IEEE Trans. Magn. 57(2):1–5
28. Ding L, Liu G, Chen Q, Xu G (2019) A novel mesh-based equivalent magnetic network for performance analysis and optimal design of permanent magnet machines. IEEE Trans. Energy Convers. 34(3):1337–1346
29. Williams CS (1936) Permanent Magnet Materials. Trans. AIEE. 55(1):19–23
30. Sun X, Shi Z, Cai Y, Lei G, Guo Y, Zhu J (2020) Driving-cycle-oriented design optimization of a permanent magnet hub

motor drive system for a four-wheel-drive electric vehicle. IEEE Trans. Transp. Electrific. 6(3):1115–1125
31. Ocak O, Aydin M (2020) An innovative semi-FEA based, variable magnet-step-skew to minimize cogging torque and torque pulsations in permanent magnet synchronous motors. IEEE Access 8:210775–210783

Junhong Wang She was born in Anhui, China, in 1999. She received the B.S. degree in electrical engineering and automation form Heilongjiang University of Science and Technology, Heilongjiang, China, in 2022. She is currently pursuing a M.S. degree at Shenyang University of Technology. Her main research direction is the electromagnetic characteristics and heat transfer analysis of axial flux permanent magnet synchronous motors .

Zengjin Xu He graduated with a M.S. degree in Mechanical Engineering from Shenyang University of Technology, in 2003 and a PhD in Mechanical Design and Theory from Shenyang University of Technology, in 2011. He is Currently a professor at the School of Electrical Engineering, Shenyang University of Technology. His research focuses on rotor dynamic characteristics evaluation and structural optimization, as well as wind power generation and photovoltaic energy storage technology .

Zuoxia Xing She graduated with a Ph.D. in Power System Automation from the School of Electrical Engineering at Beijing Jiaotong University and holds a postdoctoral position in the Department of Electrical Engineering at Tsinghua University. She is currently the Executive Dean, Professor, and Doctoral Supervisor of the New Energy Research Institute at Shenyang University of Technology. Research directions: New energy control and grid connection technology, multi energy complementarity and energy storage and consumption technology .

Yang Liu He graduated with a Ph.D. in Control Theory and Control Engineering from Northeastern University and is a postdoctoral fellow at Shenyang University of Technology. Currently, he is an Associate Professor at the School of Electrical Engineering at Shenyang University of Technology, with research interests in the operation and optimization of comprehensive energy systems, intelligent control and fault diagnosis of wind turbines, and optimization and control of electric thermal energy storage systems .

Wei Ji He was born in Anhui, China, in 1995. He received the B.S. degree in electronic Information Major of Anhui Xinhua University, Anhui, China. He is currently pursuing a M.S. degree at Shenyang University of Technology. His main research direction is the electromagnetic structure of axial flux permanent magnet synchronous motors .